# Prototype Microsolvation of Aromatic Hydrocarbon Cations by Polar Ligands: IR Spectra of Benzene$^+$−L$_n$ Clusters (L = $H_2O$, $CH_3OH$)

**Nicola Solcà and Otto Dopfer*,†**

*Department of Chemistry, University of Basel, Klingelbergstrasse 80, CH-4056 Basel, Switzerland*

*Received: October 22, 2002; In Final Form: March 7, 2003*

IR photodissociation spectra of clusters composed of the benzene cation ($Bz^+$) solvated by several water ($H_2O$=W) and methanol ($CH_3OH$=M) ligands are recorded in the O−H and C−H stretch ranges to investigate the microsolvation process of an aromatic hydrocarbon cation by polar ligands. The $Bz^+$−L (L = W, M) spectra are consistent with H-bound dimer equilibrium structures, in which the ligand L approaches $Bz^+$ in the aromatic plane to form two H-bonds between the lone pairs of the oxygen atom of L and adjacent protons of $Bz^+$. This charge−dipole structure corresponds to the global minimum of the dimer potential and is the only isomer identified in the IR spectrum. In contrast to the dimers, the spectra of larger $Bz^+$−L$_n$ clusters ($n \leq 4$ for L = W, $n \leq 2$ for L = M) provide clear evidence for the presence of two classes of isomers. Isomer class I corresponds to interior $Bz^+$ solvation and is characterized by cluster geometries in which $n$ single ligands form separate H-bonds to the central $Bz^+$ cation. Isomer class II clusters show the onset of the formation of an H-bonded solvent network, because at least one ligand forms an H-bond to a second ligand. As the $Bz^+$−L interaction is much stronger than the L−L interaction, class I isomers are probably more stable than class II isomers. Comparison between $Bz^+$−L$_n$ and Bz−L$_n$ reveals the drastic influence of ionization of the aromatic solute on both the dimer properties and the microsolvation process.

## I. Introduction

Hydration of neutral and charged molecules is a process of fundamental importance for many phenomena in chemistry and biology.[1−4] Detailed knowledge of the potential energy surface (PES) for the intermolecular interaction between the solute and solvent molecules is required to understand the effects of solvation at the molecular level. To this end, isolated size-selected clusters of the type A−L$_n$ have frequently been used as a model to characterize the stepwise microsolvation of a solute molecule (A) by an increasing and well-defined number ($n$) of ligands (L). In particular, the fruitful combination of mass spectrometric and spectroscopic techniques on the experimental side and quantum chemical tools on the theoretical side has proven to be a powerful strategy for the determination of accurate intermolecular PESs.[5] In general, the intermolecular interaction in charged complexes $A^{\pm q}$−L$_n$ is rather different from that in the corresponding neutral clusters because of the additional electrostatic, inductive, and charge-transfer contributions arising from the excess charge ($\pm q$).[6−9] The present work reports IR spectra of clusters of the benzene cation ($Bz^+$) solvated by several water (W) or methanol (M) ligands, $Bz^+$−W$_n$ and $Bz^+$−M$_n$. These clusters represent benchmark systems for the interaction of an aromatic hydrocarbon cation with polar ligands. Such interactions are relevant for biophysical phenomena where, for example, positively charged aromatic biomolecular building blocks are surrounded by a polar environment (e.g., W molecules).[3,4]

Aromatic molecules occur in nearly every facet of biochemistry, and water is the major solvent in biological systems. Consequently, neutral Bz−L$_n$ (L = W, M) complexes have attracted much interest in recent years, because they represent prototypes for neutral aromatic−hydrophilic interactions.[10−13] Extensive spectroscopic[10−16] and theoretical[14,17−21] studies have shown that Bz−W is a highly nonrigid complex. Its equilibrium structure features an archetypal $\pi$ H-bond, in which one proton of W binds to the aromatic $\pi$ electron system of Bz. Low barriers for various internal motions lead to a vibrationally averaged structure, in which both protons of W are equivalent. The most accurate measured dissociation energy, $D_0 = 2.44 \pm 0.09$ kcal/mol,[22] agrees within chemical accuracy with the value obtained at sophisticated ab initio levels, $D_0 = 2.9 \pm 0.2$ kcal/mol (MP2/fc, basis set limit).[18] IR spectra of Bz−W$_2$, Bz−W$_{3-5}$, and Bz−W$_{n\geq 6}$ have been interpreted by cluster structures, in which a W$_2$ dimer, a cyclic W$_{3-5}$ complex, or a larger three-dimensional H-bonded W$_{n\geq 6}$ network is weakly $\pi$ H-bonded to Bz, respectively.[10−13] IR spectra of all Bz−W$_n$ clusters investigated to date ($n \leq 9$)[23] have been explained with geometries in which a more or less unperturbed W$_n$ cluster is attached to one side of the aromatic Bz plane; that is, Bz is surface solvated to W$_n$.[13,24] Such Bz−W$_n$ structures are in accord with the hydrophobic character of Bz and rationalized by the fact that the W−W interaction ($D_e \approx 5$ kcal/mol)[25] is stronger than the Bz−W interaction ($D_e \approx 4$ kcal/mol).[18] In general, the H-bonds in Bz−W$_n$ tend to become stronger as the cluster size increases, reflecting the cooperative nature of the intermolecular forces in this type of cluster.[12,13] The Bz−M$_n$ structures differ in several aspects from the corresponding Bz−W$_n$ clusters, as the $CH_3$ group cannot participate in H-bonding.[10,26,27] For example, although Bz−M has also a $\pi$ H-bonded equilibrium structure, the complex is more rigid than Bz−W, because reduction of symmetry and additional steric hindrance quenches the low-barrier internal motions present in Bz−W. Moreover, Bz−M$_n$ with $n = 2$ and 3 feature chain-like M$_n$ clusters that

* Corresponding author. E-mail: dopfer@phys-chemie.uni-wuerzburg.de. Fax: +49 931 888 6378.

† Current address: Institute of Physical Chemistry, University of Würzburg, Am Hubland, D-97074 Würzburg, Germany.

10.1021/jp022286v CCC: $25.00 
Published on Web 04/24/2003

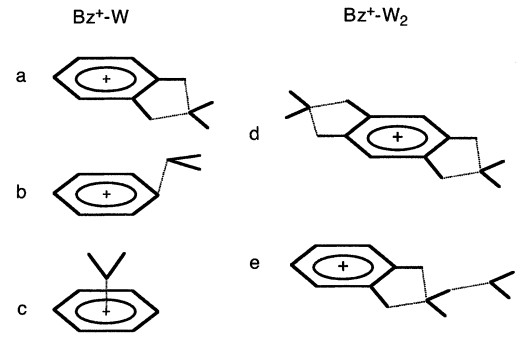


**Figure 1.** Sketch of selected structures of $Bz^+-W$ (a−c) and $Bz^+-W_2$ (d, e). The H-bound isomer of $Bz^+-W$ (a) corresponds to the global minimum on the intermolecular PES (the $Bz^+$ plane is perpendicular to the W plane), whereas the C-bound (b) and $\pi$-bound (c) dimers are less stable isomers. The two $Bz^+-W_2$ structures visualize the competition of hydration of an interior $Bz^+$ (d, isomer class I) and the formation of an H-bonded water network (e, isomer class II).

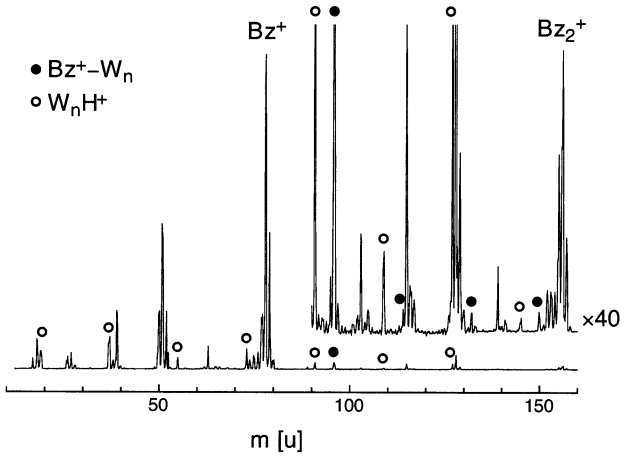


**Figure 2.** Mass spectrum of the ion source for a Bz/W/He expansion optimized for $Bz^+-W$ production. The spectrum is dominated by $Bz_n^+$ and their fragments and protonated water complexes ($W_nH^+$, open circles). $Bz^+-W_n$ complexes are indicated by filled circles. The inset is vertically expanded by a factor of 40 to show weak peaks. The relative intensities of the $Bz^+-W_n$ mass peaks decrease with $n$ as 1500:30:1:1:1 for $n = 0-4$, respectively.

are $\pi$ H-bonded to Bz, whereas only for $n > 3$ are cyclic $M_n$ subunits observed.

In contrast to neutral $Bz-W_n$ and $Bz-M_n$, theoretical and spectroscopic information about the structure and interaction strength in the corresponding cation clusters is rather sparse. Theoretical studies of $Bz^+-W$ include semiempirical[22] and quantum chemical[28−31] calculations. Three types of structures are invoked as minima on the intermolecular $Bz^+-W$ PES (Figure 1). The H-bound structure (Figure 1a), in which W approaches $Bz^+$ in the aromatic plane to form two H-bonds between the lone pairs of oxygen and adjacent protons of $Bz^+$, is calculated as the global minimum on the $Bz^+-W$ PES, with $D_e$ values ranging from 9 to 14 kcal/mol.[22,28−31] A C-bound structure (Figure 2b) with a binding energy of ≈9 kcal/mol is predicted to be a less stable isomer.[28,30] The $\pi$-bound geometry (Figure 1c) appears to be a shallow local minimum[22] with $D_e \approx 7 \pm 1$ kcal/mol.[22,31] All three structures are mainly stabilized by the charge−dipole attraction between the positive charge distribution in $Bz^+$ and the dipole moment of W. Hence, they are characterized by charge−dipole configurations, in which the oxygen of W points toward the $Bz^+$ charge. Very recently, IR spectra of $Bz^+-W$ produced in a supersonic expansion provided the first spectroscopic information about the structure and dissociation energy of this important dimer.[30,31] By comparison with quantum chemical calculations, the analysis of the frequencies and IR intensities of the O−H and C−H stretch vibrations demonstrates that the calculated H-bound geometry shown in Figure 1a corresponds indeed to the most stable $Bz^+-W$ structure. The vibrational and isomer assignments are further confirmed by IR spectra of $Bz^+-HDO$ and $Bz^+-W-N_2$.[31] Moreover, the dissociation energy estimated from the frequency shifts of the O−H stretch fundamentals of W, $D_0 = 14 \pm 3$ kcal/mol,[31] is consistent with the $D_e$ values of 9−14 kcal/mol calculated for the H-bound structure. The IR spectra do not show any evidence for the presence of other less stable $Bz^+-W$ isomers in the expansion, which is attributed to their significantly lower stabilization energies and/or low isomerization barriers toward the most stable H-bound minimum.[31]

Comparison between Bz−W and $Bz^+-W$ demonstrates that ionization of the aromatic solute has drastic effects on the topology of the intermolecular PES, including both the structure and interaction energy of the global minimum.[22,28−31] In the present work, IR spectra of $Bz^+-W_n$ ($n = 2-4$) and $Bz^+-M_n$ ($n = 1, 2$) are reported and analyzed for the first time, with the major goal of extending the initial $Bz^+-W$ studies toward complexes with other polar ligands and a larger number of solvent molecules. To the best of our knowledge, neither spectroscopic nor theoretical information is available for these clusters. For the corresponding neutral complexes, structural information has mainly been derived from IR spectra in the O−H and C−H stretch ranges, which provide a sensitive probe of the details of the geometry of the H-bonded ligand network.[10−13] A similar strategy is thus followed here for $Bz^+-L_n$ (L = W, M). Of particular interest are the effects of the positive charge on the structure of the first solvation shell, including the competition between microsolvation of an interior $Bz^+$ cation and the formation of an H-bonded solvent cluster network ($L_n$). As the $Bz^+-L$ interaction is significantly stronger than the L−L interaction, the most stable $Bz^+-L_n$ clusters are expected to have structures in which the ligands L are solvated around an interior $Bz^+$ cation. This is in striking contrast to neutral $Bz-L_n$ clusters, which prefer geometries in which Bz is attached to the surface of a $L_n$ network. Moreover, induction forces are highly nonadditive and provide a significant contribution to the interaction in charged complexes.[6,32] Thus, the presented $Bz^+-L_n$ spectra probe also the degree of (non)-cooperativity of the three-body interactions in this type of clusters. Previous mass spectrometric studies have shown that $Bz^+-W_n$ ($n \leq 7$) and $Bz^+-M_n$ ($n \leq 2$) produced by photoionization do not undergo intracluster ion−molecule reactions.[24,33] Hence, although chemical reactions have been observed for larger clusters (e.g., proton or electron transfer),[24,33] the $Bz^+-L_n$ complexes in the size range considered in the present work are expected to be unreactive with respect to intracluster reactions.

## II. Experimental Section

IR spectra of mass selected $Bz^+-W_n$, $Bz^+-W-N_2$, and $Bz^+-M_n$ clusters are recorded in a tandem mass spectrometer coupled to a cluster ion source and an octopole ion trap. The ion source combines electron impact ionization with a molecular beam expansion. The expanding gas mixture is produced by bubbling either He or $N_2$ buffer gas at room temperature and 4−8 bar stagnation pressure through two successive reservoirs filled with water (or methanol) and benzene. Electron impact ionization ($E \approx 10^2$ eV) close to the nozzle orifice and subsequent clustering reactions in the high-pressure region of

the adiabatic expansion produce (cluster) ions in the supersonic plasma jet. The main production pathway of $Bz^+-L_n$ clusters starts with chemical ionization of Bz (Penning or electron impact ionization) and subsequent three-body association reactions according to:

$$Bz + e^- \rightarrow Bz^+ + 2e^- \quad (1a)$$

$$Bz^+-L_{n-1} + L + X \rightarrow Bz^+-L_n + X \quad (1b)$$

The ligand L in reaction step 1b may also be replaced by a larger neutral solvent cluster $L_p$. In this case, stabilization of the intermediate cluster occurs by three-body association or evaporative cooling:

$$Bz^+-L_{n-p} + L_p + X \rightarrow Bz^+-L_n + X \quad (1c)$$

$$Bz^+-L_{n+m-p} + L_p \rightarrow Bz^+-L_n + mL \quad (1d)$$

An alternative path for the generation of $Bz^+-L_n$ clusters begins with the formation of neutral $Bz-L_{n+m}$ clusters in the initial part of the expansion, followed by ionization and evaporative (and/or collisional) cooling:

$$Bz-L_{n+m} + e^- \rightarrow (Bz^+-L_{n+m})^* + 2e^- \rightarrow Bz^+-L_n + mL + 2e^- \quad (2)$$

Previous experiments on related cluster systems clearly demonstrate that reaction 1 corresponds to the dominant production mechanism in the present ion source. In particular for dimers ($n = 1$), reaction 1b generates predominantly the most stable cluster isomer of $Bz^+-L$.[31,34−37] On the other hand, the generation of larger $Bz^+-L_n$ clusters via reaction 1 may not exclusively be controlled by thermodynamic considerations, because kinetic factors can also influence the isomer distribution. Consequently, in addition to the most stable $Bz^+-L_n$ clusters, less stable isomers may be produced with significant abundance as well. A mass spectrum of the ion source for a typical Bz/W/He expansion is presented in Figure 2. In this particular case, the parameters of the ion source are optimized for the production of the $Bz^+-W$ dimer. The spectrum is dominated by $Bz_n^+$ and their fragment ions[38,39] as well as protonated water complexes ($W_nH^+$, open circles). The $Bz^+-W_n$ series is indicated by filled circles.

The central part of the supersonic plasma is extracted from the ion source chamber through a skimmer into an initial quadrupole mass spectrometer (QMS1), which is tuned to the mass of the parent cluster under investigation. The mass selected ion beam is then focused into an octopole ion guide, where it interacts with a tunable IR laser pulse. Resonant excitation of metastable vibrational levels above the lowest dissociation threshold causes the cleavage of the weakest intermolecular bond:

$$Bz^+-L_n + \nu_{IR} \rightarrow Bz^+-L_{n-1} + L \quad (3a)$$

$$Bz^+-L_n-N_2 + \nu_{IR} \rightarrow Bz^+-L_n + N_2 \quad (3b)$$

Only the loss of a single ligand is observed under the present experimental conditions. The produced fragment ions are selected by a second quadrupole mass spectrometer (QMS2) and monitored with a Daly ion detector as a function of the laser frequency ($\nu_{IR}$) to obtain the IR action spectra of the parent clusters. As an example, Figure 3 shows the mass spectra

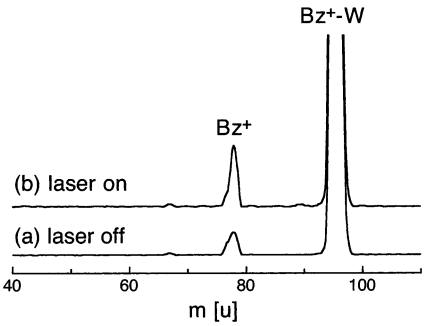


**Figure 3.** Mass spectra obtained by mass selecting $Bz^+-W$ with QMS1 and scanning QMS2 to monitor metastable decay and laser induced dissociation in the octopole: (a) the laser is off and the $Bz^+$ fragment ions (≈4% of $Bz^+-W$) arise solely from metastable decay of $Bz^+-W$; (b) the laser is tuned to a strong resonance of $Bz^+-W$ ($\nu_{IR} = \nu_1^W = 3637$ cm$^{-1}$), and additional $Bz^+$ fragment ions (≈6% of $Bz^+-W$) originate from laser induced dissociation.

obtained by mass selecting $Bz^+-W$ with QMS1 and scanning QMS2 without (a) and with (b) resonant IR excitation. The $Bz^+$ fragment ions (≈4% of $Bz^+-W$) in spectrum (a) are produced by metastable decay of hot $Bz^+-W$ ions in the octopole. Spectrum (b) reveals additional fragmentation of $Bz^+-W$ (≈6%) arising from resonant excitation of a strong vibrational resonance ($\nu_{IR} = \nu_1^W = 3637$ cm$^{-1}$). To separate the metastable decay from laser-induced dissociation, the ion source is triggered at twice the laser frequency, and signals from alternating triggers are subtracted. Tunable IR radiation with 0.02 cm$^{-1}$ bandwidth is generated by a pulsed optical parametric oscillator laser system pumped by a seeded Nd:YAG laser. Calibration of the IR laser frequency, accurate to better than 1 cm$^{-1}$, is accomplished by optoacoustic spectra of HDO and $NH_3$,[40] as well as atmospheric water absorptions along the IR laser path.[41] All IR spectra are linearly normalized for laser intensity variations measured with an InSb detector.

## III. Results and Discussion

IR photodissociation spectra of $Bz^+-W_n$ ($n = 1-4$), $Bz^+-W-N_2$, and $Bz^+-M$ recorded in the O−H stretch range are compared in Figure 4. Corresponding IR spectra of $Bz^+-W$, $Bz^+-W-N_2$, and $Bz^+-M$ obtained in the vicinity of the C−H stretch vibrations are reproduced in Figure 5. The maxima and widths of the observed bands (denoted A−H) are listed in Table 1, along with their vibrational and isomer assignments.

**A. $Bz^+-W$ and $Bz^+-W-N_2$.** As most parts of the IR spectra of $Bz^+-W$ and $Bz^+-W-N_2$ have been discussed previously,[30,31] only the salient results are summarized here. The $Bz^+-W$ spectrum in the O−H stretch range (Figure 4) is characterized by two intense bands B and A centered at 3637 and 3718 cm$^{-1}$, respectively.[31] On the basis of their frequencies and relative intensities, they are assigned to the symmetric and antisymmetric O−H stretch modes ($\nu_1^W$, $\nu_3^W$) of the W ligand in H-bound $Bz^+-W$ (Figure 1a). The modest red shifts of $\Delta\nu_1^W = -20$ cm$^{-1}$ and $\Delta\nu_3^W = -38$ cm$^{-1}$ with respect to the W monomer transitions ($\nu_1^W = 3657$ cm$^{-1}$, $\nu_3^W = 3756$ cm$^{-1}$)[42] indicate that both O−H bonds are hardly perturbed by complexation and are not involved in intermolecular H-bonding. In contrast to the frequencies, the presence of $Bz^+$ strongly affects the relative IR intensities of $\nu_1^W$ and $\nu_3^W$. In isolated W, $\nu_3^W$ is much more intense than $\nu_1^W$,[42] whereas in $Bz^+-W$ both transitions have comparable IR oscillator strengths. Comparison with quantum chemical calculations shows that the observed intensity and frequency changes are fully consistent with an assignment to the H-bound charge−dipole complex in Figure

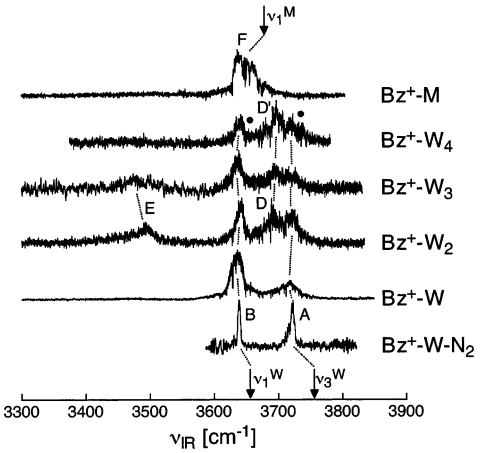


**Figure 4.** IR photodissociation spectra of $Bz^+-W-N_2$, $Bz^+-W_n$ ($n = 1-4$), and $Bz^+-M$ in the O−H stretch range. The $Bz^+-W-N_2$ spectrum is recorded in the $Bz^+-W$ fragment channel, whereas those of $Bz^+-W_n$ and $Bz^+-M$ are measured in the $Bz^+-W_{n-1}$ and $Bz^+$ fragment channels, respectively. The positions and assignments of the bands observed are listed in Table 1. Corresponding transitions are connected by dotted lines. The arrows indicate the symmetric and antisymmetric O−H stretch vibrations of bare W ($\nu_1^W = 3657$ cm$^{-1}$, $\nu_3^W = 3756$ cm$^{-1}$),[42] as well as the O−H stretch fundamental of bare M ($\nu_1^M = 3681$ cm$^{-1}$).[57] Narrow dips between 3600 and 3800 cm$^{-1}$ are due to atmospheric water absorptions along the IR laser path. The signals marked by filled circles correspond possibly to $Bz^+-W_4$ isomers with C-bound and/or $\pi$-bound W ligands.

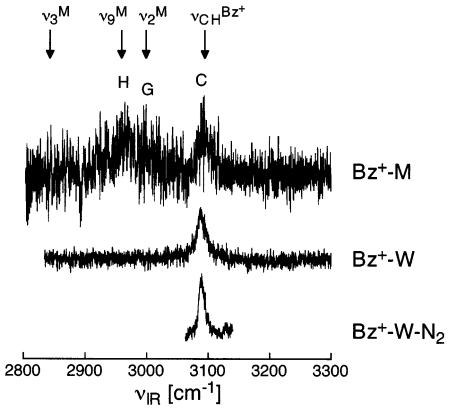


**Figure 5.** IR photodissociation spectra of $Bz^+-W-N_2$, $Bz^+-W$, and $Bz^+-M$ in the C−H stretch range. The $Bz^+-W-N_2$ spectrum is recorded in the $Bz^+-W$ fragment channel, whereas those of $Bz^+-W$ and $Bz^+-M$ are measured in the $Bz^+$ fragment channel. The positions and assignments of the bands observed are listed in Table 1. The arrows indicate the intense C−H stretch band of bare $Bz^+$ estimated from $Bz^+-Rg$ spectra ($\nu_{20}^{Bz^+}$ and/or $\nu_{13}^{Bz^+}$ at ≈3095 cm$^{-1}$),[44,46,73] as well as the C−H stretch fundamentals of bare M ($\nu_2^M = 3000$ cm$^{-1}$, $\nu_3^M = 2844$ cm$^{-1}$, $\nu_9^M = 2960$ cm$^{-1}$).[57]

1a.[30,31] Moreover, the binding energy estimated from the frequency shifts, $D_0 = 14 \pm 3$ kcal/mol,[31] is in good agreement with the values calculated for this isomer (9−14 kcal/mol).[22,28−31] The spectrum of $Bz^+-HDO$ shows only a single band in the O−H stretch range, at a frequency (3679 cm$^{-1}$) approximately midway between the two O−H stretch vibrations of $Bz^+-H_2O$.[31] This observation confirms the interpretation that the two bands in the $Bz^+-H_2O$ spectrum arise indeed from $\nu_1^W$ and $\nu_3^W$ of a single $Bz^+-W$ isomer, and not from single transitions of two different structural isomers. The red shift of the O−H stretch in $Bz^+-HDO$ with respect to free HDO (3707 cm$^{-1}$)[42] amounts to −28 cm$^{-1}$. The small red shifts of the O−H stretch modes in $Bz^+-H_2O$ and $Bz^+-HDO$ imply that the strength of the O−H bonds is slightly reduced upon $Bz^+$ complexation; that is, the O−H bonds appear to be more acidic in the complex. Moreover, the red shifts reflect directly the increase of the intermolecular bond strength upon O−H stretch excitation. Assuming a ground-state dissociation energy of the order of ≈5000 cm$^{-1}$,[31] the small red shifts of the O−H stretch modes (20−40 cm$^{-1}$) imply that vibrational excitation enhances the interaction by 0.4−0.8%. As expected for a charge-dipole orientation, the stretch modes of the free O−H bonds in the H-bound $Bz^+-W$ dimer couple only weakly to the intermolecular degrees of freedom. Interestingly, while the Bz−W spectrum is complicated by large splittings arising from only slightly hindered internal motions,[12,43] the $Bz^+-W$ spectrum does not display such splittings, indicating that internal W motions are largely quenched by significant barriers in the cation dimer.[30]

The IR spectrum of $Bz^+-W$ in the C−H stretch range displays a single band centered at 3088 cm$^{-1}$ (band C in Figure 5) which is assigned to $\nu_{20}^{Bz^+}$ and/or $\nu_{13}^{Bz^+}$. The corresponding frequency of this band in isolated $Bz^+$ may be estimated from the IR spectra of weakly $\pi$-bound $Bz^+-L$ dimers (L = Ne, Ar, $N_2$, $CH_4$) as ≈3095 cm$^{-1}$.[44−46] Thus, the formation of the two nonlinear C−H···O H-bonds to W has a surprisingly small effect on the frequency of the C−H stretch, with a red shift of less than 10 cm$^{-1}$. However, its IR intensity is considerably enhanced upon hydration of $Bz^+$, and this effect has been taken as strong evidence for the formation of the C−H···O H-bonds, which confirms the assignment to the H-bound $Bz^+-W$ structure in Figure 1a.[30] Again, the spectral observations in the C−H stretch range are well reproduced by quantum chemical calculations for H-bound $Bz^+-W$.[30]

The $Bz^+-HDO$ spectrum clearly shows that only one $Bz^+-W$ isomer contributes to the IR spectrum observed. However, the detected isomer may not necessarily correspond to the global minimum because the photon energy is insufficient for dissociation of the most stable $Bz^+-W$ structure from the ground vibrational state. For example, the ab initio binding energy of H-bound $Bz^+-W$ ($D_e \approx 4500-4800$ cm$^{-1}$)[28,31] exceeds the fundamental O−H stretch frequencies, whereas that predicted for the $\pi$-bound isomer ($D_e \approx 2200$ cm$^{-1}$)[31] is smaller than these vibrational energies. The low laser intensities available in the present experiment (<200 kW/cm$^2$) exclude multiphoton processes.[31] Hence, assuming single-photon absorption from the ground vibrational state, the most stable H-bound isomer may not be observed in the $Bz^+-W$ photodissociation spectrum, whereas the $\pi$-bound isomer could be detected. To test how many $Bz^+-W$ isomers are indeed produced in the supersonic plasma expansion, IR spectra of $Bz^+-W-N_2$ are recorded in the $Bz^+-W$ channel (eq 3b). All $Bz^+-W$ isomers should contribute to a single photon photofragmentation spectrum of $Bz^+-W-N_2$ because the binding energy of $N_2$ to any $Bz^+-W$ structure (<3 kcal/mol) is well below the O−H and C−H stretch frequencies.[34,35,37,44] Similar to $Bz^+-W$, the $Bz^+-W-N_2$ spectrum displays only three (narrow) bands in the O−H and C−H stretch ranges (Figures 4 and 5), confirming that only one $Bz^+-W$ isomer is present with significant abundance in the employed ion source. As this source produces predominantly the most stable isomer of a given dimer ion (eq 1b),[31,34−37] all transitions of $Bz^+-W$ and $Bz^+-W-N_2$ have to be attributed to the H-bound $Bz^+-W$ structure shown in Figure 1a. The fact that the vibrational frequencies of H-bound $Bz^+-W$ are below its dissociation energy implies that the observed bands do not correspond to fundamental transitions from the ground vibrational state ($\nu_i$). Instead, they arise from sequence hot bands of the type $\nu_i + \nu_x \leftarrow \nu_x$ of "warm" $Bz^+-W$ clusters where $\nu_i$

**TABLE 1: Frequencies and Widths (fwhm, in parentheses) of the Transitions Observed in the IR Spectra of $Bz^+-W_n$ ($n$ = 1−4), $Bz^+-W-N_2$, and $Bz^+-M_n$ ($n$ = 1, 2), along with Their Vibrational and Isomer Assignments**

| peak | $Bz^+-W$ | $Bz^+-W-N_2$ | $Bz^+-W_2$ | $Bz^+-W_3$ | $Bz^+-W_4$ | $Bz^+-M$ | $Bz^+-M_2$ | assignment[b] |
|---|---|---|---|---|---|---|---|---|
| A | 3718 (20)[a] | 3722 (8)[a] | 3724 (15) | 3721 (16) | 3727 (23) | | | $\nu_3^W$ (I) |
| B | 3637 (20)[a] | 3639 (5)[a] | 3642 (15) | 3635 (16) | 3640 (20) | | | $\nu_1^W$ (I) |
| C | 3088 (17) | 3089 (11) | | | | 3090 (20) | | $\nu_{13}/\nu_{20}^{Bz+}$ (I) |
| D | | | 3691 (14) | 3697 (19) | 3697 (17) | | | free $\nu_{OH}$ (II) |
| D′ | | | | | 3677 (20) | | | free $\nu_{OH}$ (II) |
| E | | | 3494 (44) | 3479 (43) | | | | bound $\nu_{OH}$ (II) |
| F | | | | | | 3650 (40) | 3655 (30) | $\nu_1^M$ (I) |
| G | | | | | | 3005 (30) | | $\nu_2^M$ (I) |
| H | | | | | | 2965 (30) | | $\nu_9^M$ (I) |

[a] Reference 31. [b] Isomer I corresponds to hydrated $Bz^+$ without any W−W (or M−M) bond, whereas isomer II corresponds to structures with a water network.

$+ \nu_x$ exceeds $D_0$ of $Bz^+-W$.[31] The bands of $Bz^+-W-N_2$ are much narrower (5−11 $cm^{-1}$) than those of $Bz^+-W$ (17−20 $cm^{-1}$), confirming that the effective rotational and vibrational temperatures are much lower in the former spectrum. In contrast to the widths, the vibrational frequencies of $Bz^+-W-N_2$ are similar to those of $Bz^+-W$ with deviations of less than 5 $cm^{-1}$. Consequently, the $Bz^+-W-N_2$ spectrum resembles closely the one of "cold" $Bz^+-W$, consistent with the weak interaction between $Bz^+-W$ and $N_2$.[34,35,37,44] Moreover, the small shifts imply that the couplings between the O−H/C−H stretch fundamentals and $\nu_x$ are weak. This observation suggests that $\nu_x$ are predominantly low-frequency $Bz^+$ vibrations and their combination bands with intermolecular modes. The major effect of the $N_2$ ligand is thus to reduce the effective temperature and the dissociation energy required to cleave the weakest intermolecular bond. Unfortunately, this useful messenger technique could only be applied to $Bz^+-W$ in the present work because of the low production of other $Bz^+-L_n-N_2$ clusters.

**B. $Bz^+-W_2$.** The IR spectrum of $Bz^+-W$ clearly demonstrates that the H-bound isomer in Figure 1a is the most stable structure of this dimer, with a dissociation energy of $D_0$ = 14 ± 3 kcal/mol. On the other hand, $W_2$ has an H-bonded equilibrium structure, in which one H atom of the proton donor forms a nearly linear H-bond to the O atom of the proton acceptor.[47,48] The best experimental value for the $W_2$ binding energy is probably $D_0$ = 3.34 ± 0.7 kcal/mol.[49,50] Thus, the W−W interaction is roughly four times weaker than the $Bz^+-W$ interaction. Consequently, the most stable $Bz^+-W_2$ structure is expected to be one in which two single W molecules form separate H-bonds to $Bz^+$. An example of such a structure representing $Bz^+$ hydration (denoted isomer class I) is shown in Figure 1d. $Bz^+$ offers six H-bonding sites for W ligands, implying that the first "planar" hydration subshell around an interior $Bz^+$ is closed for $Bz^+-W_6$. The sequence of filling this subshell is not obvious, and several isomers lying close in energy may exist. In these $Bz^+-W_n$ structures, the individual W ligands are (nearly) equivalent and the interaction between the ligands is much smaller than the interaction with the central cation. Hence, the mid-IR spectra of these class I isomers are expected to closely resemble that of the H-bound $Bz^+-W$ dimer. Indeed, the $Bz^+-W_2$ spectrum in Figure 4 shows two intense bands in the O−H stretch range (A and B) which are close to the corresponding absorptions of $Bz^+-W$. They are attributed to the antisymmetric and symmetric O−H stretch modes of the W ligands ($\nu_3^W$ and $\nu_1^W$) in $Bz^+-W_2$. Closer inspection reveals that their band centers at 3724 and 3642 $cm^{-1}$ demonstrate small but noticeable blue shifts of 6 and 5 $cm^{-1}$ compared to the corresponding $Bz^+-W$ bands, indicating that the intermolecular H-bonds in $Bz^+-W_2$ are significantly weaker than in $Bz^+-W$. These blue shifts reduce the absolute red shifts induced by the first ligand in $Bz^+-W$ (−38 and −20 $cm^{-1}$) by 16% and 25%, respectively, emphasizing the remarkable influence of the second ligand on the interaction with the first ligand. Several factors may contribute to this large noncooperative effect. First, the (permanent and induced) dipole moments ($\mu$) of the W ligands are not aligned in an optimal $\mu-\mu$ orientation. For example, the dipole moments of the two ligands in the specific $Bz^+-W_2$ structure shown in Figure 1d point in opposite directions, corresponding to an unfavorable $\mu-\mu$ interaction.[32] In total, three different configurations are possible for arranging two W ligands around the $Bz^+$ cation plane: their dipoles can include angles of roughly 60° (ortho), 120° (meta), or 180° (para, Figure 1d). Modeling the $\mu-\mu$ interaction ($V$) for the three orientations (assuming 4 Å for the intermolecular $Bz^+-W$ center-of-mass separation)[31] yields $V/V_0$ = +0.031, +0.037, and +0.078 for the 180°, 120°, and 60° structures, respectively ($V_0 \sim \mu^2$). Thus, all orientations provide a repulsive contribution of the $\mu-\mu$ interaction to the total binding energy (noncooperative effect). Moreover, the 180° and 120° configurations are similar in energy and more stable than the 60° isomer. In addition to the $\mu-\mu$ interaction, structural reorganization of $Bz^+$ upon sequential hydration may contribute to the observed noncooperativity in $Bz^+-W_2$. Complexation of $Bz^+$ by the first W causes significant changes of the structure of $Bz^+$. For example, the compressed form of isolated $Bz^+$ (which is Jahn−Teller distorted in its $^2E_{1g}$ electronic ground state)[51−53] is calculated to be slightly more stable than the elongated form, whereas the reverse situation is predicted for $Bz^+-W$.[29] It is likely that the structural reorganization of $Bz^+$ induced by the first W is not favorable for the interaction with the second W, causing a decrease in the average ligand binding energy in $Bz^+-W_2$. Moreover, the widths of the $Bz^+-W_2$ transitions (15 $cm^{-1}$) are smaller than those of the corresponding $Bz^+-W$ bands (20 $cm^{-1}$), providing further evidence that the intermolecular bonds in $Bz^+-W_2$ are weaker than in $Bz^+-W$. To cleave weaker bonds by IR absorption requires less internal energy prior to photoexcitation and, as a consequence, photodissociation spectra with lower effective rotational and vibrational temperatures are obtained.

In addition to bands A and B, which by comparison with the $Bz^+-W$ spectrum are assigned to $\nu_3^W$ and $\nu_1^W$ of a $Bz^+$ hydrated $Bz^+-W_2$ structure (isomer class I, Figure 1d), the spectrum of $Bz^+-W_2$ displays two additional bands (D and E) in the O−H stretch range at 3691 and 3494 $cm^{-1}$ that are not present in the $Bz^+-W$ spectrum (Figure 4). The latter bands are assigned to a second $Bz^+-W_2$ isomer, in which a perturbed $W_2$ dimer is connected to the $Bz^+$ cation via bifurcated H-bonding (isomer class II, Figure 1e). Band E at 3494 $cm^{-1}$ displays a large red shift of −213 $cm^{-1}$ from the average O−H stretch frequency of isolated W (3707 $cm^{-1}$) and provides thus clear evidence that one of the W molecules in the considered $Bz^+-W_2$ isomer acts as a proton donor in an H-bond. The equilibrium structure

of $W_2$ features a nearly linear O−H···O H-bond; that is, one W acts as the proton donor and the other one as the proton acceptor.[47,48] The frequencies of three of the four O−H stretch modes of $W_2$ were determined as 3735 (free donor stretch), 3601 (bound donor stretch), and 3745.5 $cm^{-1}$ (antisymmetric acceptor stretch).[47,54] The symmetric acceptor stretch with an estimated frequency of 3655−3660 $cm^{-1}$ has not been observed because of its low IR intensity.[54] Hence, by comparison with the $W_2$ frequencies, band E at 3494 $cm^{-1}$ in $Bz^+-W_2$ is assigned to the bound O−H stretch of the proton donor of $W_2$ attached to $Bz^+$. Significantly, for $Bz^+-W_2$ the red shift from the average O−H stretch frequency of free W (−213 $cm^{-1}$) is twice that of $W_2$ (−106 $cm^{-1}$). Hence, the presence of $Bz^+$ drastically enhances the strength of the H-bond in the $W_2$ moiety. This large cooperative three-body effect is not surprising because $Bz^+$ increases the acidity of the O−H bonds of the first W ligand, as is deduced from the red shifts $\Delta\nu_1^W$ and $\Delta\nu_3^W$ of $Bz^+-W$. Moreover, the positive charge in $Bz^+$ increases the effective dipole moment of the first W (by charge-induced dipole interaction), which in turn provides an additional contribution to the W−W interaction in $Bz^+-W_2$. Band D at 3691 $cm^{-1}$ in the $Bz^+-W_2$ spectrum is attributed to a free O−H stretch of isomer II. As described before, the three free O−H stretch modes of $W_2$ have frequencies of ≈3660 (symmetric acceptor stretch), 3735 (free donor stretch), and 3745.5 $cm^{-1}$ (antisymmetric acceptor stretch), but only the latter two have significant IR intensities.[47,54] Although an unambiguous assignment of band D to a specific free O−H stretch mode in $Bz^+-W_2$ is impossible at the present stage, an assignment to the free O−H stretch of the donor appears most probable. Complexation with $Bz^+$ reduces the O−H bond strength in the donor and explains that the frequency of this mode in $Bz^+-W_2$ is lower than in bare $W_2$ (3691 vs 3735 $cm^{-1}$). On the other hand, an assignment of band D to the symmetric acceptor stretch in $Bz^+-W_2$ appears unlikely, because $Bz^+$ complexation strengthens the W−W interaction and should reduce the frequency of this mode compared to its value in bare $W_2$ (≈3660 $cm^{-1}$). Thus, this mode may actually contribute to band B (centered at 3642 $cm^{-1}$), which is mainly attributed to the intense $\nu_1^W$ transition of class I isomers of $Bz^+-W_2$. (Although the IR intensity of the symmetric acceptor stretch in $W_2$ is rather low,[54] the corresponding transition in $Bz^+-W_2$ may be observed as $Bz^+$ complexation can have a drastic effect[29−31] on the relative intensities of certain normal modes of surrounding W ligands.) An alternative assignment of band D to the antisymmetric acceptor stretch in $Bz^+-W_2$ may also be excluded because this interpretation would imply red shifts of −55 and −65 $cm^{-1}$ compared to $W_2$ and W, respectively. However, the W−W interaction in $Bz^+-W_2$ is probably not strong enough to cause such large shifts in the acceptor stretch modes. For example, the strong $Bz^+-W$ bond ($D_0$ = 14 ± 3 kcal/mol), which is almost certainly more stable than the W−W bond in $Bz^+-W_2$, induces only a shift of −38 $cm^{-1}$ of $\nu_3^W$ in $Bz^+-W$. Nonetheless, as the W−W interaction is enhanced by the presence of $Bz^+$, the acceptor stretch modes of $Bz^+-W_2$ are expected to have lower frequencies than in $W_2$. Most likely, the antisymmetric acceptor stretch (3745.5 $cm^{-1}$ in $W_2$) is blended by the intense $\nu_3^W$ transition of class I isomers of $Bz^+-W_2$ (band A at 3724 $cm^{-1}$). In addition to the frequencies, the rather different widths of bands E (44 $cm^{-1}$) and D (14 $cm^{-1}$) support their assignments to bound and free O−H stretch modes, respectively. Proton donor stretch vibrations couple more strongly to the intermolecular degrees of freedom, giving rise to a broader band contour.[6] On the other hand, this coupling is weaker for free O−H stretch modes (of both isomer types), leading to correspondingly narrower transitions.[6]

The analysis of the IR spectrum of $Bz^+-W_2$ in the O−H stretch range clearly reveals the spectroscopic fingerprints of two classes of isomers, namely isomer class I corresponding to $Bz^+$ hydration (Figure 1d) and isomer class II corresponding to the formation of a solvent network (Figure 1e). On the basis of the dimer interactions alone ($D_0$ = 14 ± 3 and 3.34 ± 0.7 kcal/mol for $Bz^+-W$ and W−W, respectively), isomers I are predicted to be much more stable than isomer II (by ≈11 kcal/mol). On the other hand, cooperative and noncooperative (three-body) effects are observed to become important for both isomer classes as the number of ligands in the cluster is increased. Apparently, these are extremely cooperative for the W−W bond in isomer II of $Bz^+-W_2$, whereas they are significantly noncooperative for the $Bz^+-W$ bond in isomer I of $Bz^+-W_2$. Consequently, the difference in the stability of both types of isomers is possibly much smaller than predicted by the dimer bond strengths alone. It is difficult to estimate their relative stability from the experimental spectra, because several factors influence the observed IR intensities. First, photodissociation spectra do not directly reflect the absorption cross section but correspond to the product of absorption and dissociation cross sections. The latter may sensitively depend on the type of isomer (and also on the type of vibration) because of different dissociation energies and predissociation dynamics. For example, the signals of an isomer with lower binding energy and larger dissociation rates will be enhanced compared to those from another isomer with a stronger bond and lower dissociation rates. Moreover, the IR intensities are difficult to analyze in a quantitative fashion because the contributions of sequence hot bands and fundamental transitions cannot easily be separated. In addition, reliable quantum chemical calculations of IR intensities are challenging for complexes composed of $Bz^+$ because of the degeneracy of its $^2E_{1g}$ electronic ground state and the resulting dynamic Jahn−Teller distortion.[29,52] Such calculations are, however, required for a quantitative analysis of the O−H stretch intensities, because $Bz^+$ complexation has a large effect on the IR intensities of certain W vibrations.[29−31] Finally, even if it were possible to reliably extract the relative abundance of both isomer types from the IR spectra, it would not be possible to use this information to evaluate their relative stability because their concentration in the molecular beam is not only controlled by thermodynamic considerations. The competing production schemes described in eq 1(a−d) suggest that kinetic factors may also play a significant role in the determination of the production ratio of certain isomers. For example, isomers I of $Bz^+-W_2$ are predominantly produced by sequential three-body association of two single W ligands to $Bz^+$ (eq 1b). Similarly, isomer II of $Bz^+-W_2$ can be generated via this route, although the probability for the second W to bind to the first W of $Bz^+-W$ is much lower than binding to $Bz^+$ from both energetic and entropic arguments. However, significant concentrations of isomer II of $Bz^+-W_2$ may also be produced by attaching a preformed neutral water cluster to $Bz^+$ with subsequent stabilization by collisional or evaporative cooling (eq 1c,d). The relative importance of the different production pathways depends on the expansion conditions and may lead to isomer concentrations that are rather different from those predicted by thermodynamic considerations alone.

**C. $Bz^+-W_{3,4}$.** In general, the $Bz^+-W_3$ spectrum recorded in the O−H stretch range is similar in appearance to the $Bz^+-W_2$ spectrum (Figure 4). In particular, it reveals also the spectroscopic fingerprints of both classes of isomers. Isomer

type I corresponds to hydration of an interior $Bz^+$, with three single W ligands forming separate H-bonds to the central cation. Bands A and B centered at 3721 and 3635 $cm^{-1}$ are assigned to $\nu_3^W$ and $\nu_1^W$ of these W ligands. Their frequencies are close to those of $Bz^+-W$ and the corresponding isomer type I of $Bz^+-W_2$, confirming that there is relatively little coupling between the individual W ligands in this type of $Bz^+-W_n$ isomer with interior ion solvation. Again, three structural configurations with similar binding energies (and IR spectra) are expected, which differ just in the way the three W ligands occupy the six available H-bonding sites offered by $Bz^+$.

Similar to $Bz^+-W_2$, the IR spectrum of $Bz^+-W_3$ displays a broad band E in the low-frequency O−H stretch range (centered at 3479 $cm^{-1}$), which clearly indicates the presence of an isomer in which (at least) one W ligand acts as a proton donor. Moreover, the narrower band D assigned to isomer type II of $Bz^+-W_2$ occurs again in the $Bz^+-W_3$ spectrum (at 3697 $cm^{-1}$). Consequently, bands D and E are both attributed to free and bound O−H stretch modes of various isomer type II structures, which show at least the onset of the formation of a water ligand network. Several structures may be considered. Probably the most stable type II isomers are those which have a $W_2$ dimer and a single W molecule separately attached to two of the six available H-bonding sites of $Bz^+$. These isomers are expected to have similar O−H stretch spectra of $Bz^+-W_2$ (type I plus type II), as the $W_2$ unit is not interacting much with the third W ligand. A second group of presumably less stable type II isomers is characterized by geometries in which a $W_3$ complex is linked to the $Bz^+$ cation. The $W_3$ complex can have either a chain-like structure, with the terminal W ligand forming an H-bond to $Bz^+$, or a branched configuration, in which two single W ligands are H-bonded to the two protons of the first W ligand.[55] The branched structure is likely to be more stable than the chained one, because of the shorter average separation of the W ligands from the $Bz^+$ charge. In contrast to isolated cyclic $W_3$,[56] a $Bz^+-W_3$ structure with a $W_3$ ring appears to be an unfavorable configuration because one W ligand needs to act as a double donor in the latter system. The quality of the $Bz^+-W_3$ spectrum is insufficient to determine which specific type II isomer is actually present in the expansion.

The $Bz^+-W_4$ spectrum features also the absorptions of type I and type II isomers (Figure 4). Bands A and B at 3727 and 3640 $cm^{-1}$ are assigned to $\nu_3^W$ and $\nu_1^W$ of isomer type I with four single W ligands attached to an interior $Bz^+$ ion. Bands D and D′ at 3697 and 3677 $cm^{-1}$ are again indicative of free O−H stretch modes of type II isomers in which at least one W ligand is a proton donor. Interestingly, the corresponding signals of the bound O−H stretches near 3500 $cm^{-1}$ (band E) are not observed, possibly because of the low signal-to-noise levels achieved. In general, the increasing congestion and widths of the bands in the O−H stretch range of the $n = 3$ and 4 spectra suggest that, with increasing cluster size, more and more $Bz^+-W_n$ isomers contribute to the IR spectra. As solvation proceeds, the probability for the presence of isomers featuring C-bound or $\pi$-bound W ligands in the expansion is increasing as well. Such ligands should have $\nu_1^W$ and $\nu_3^W$ absorptions to the blue of bands B and A of H-bound $Bz^+-W$ due to the weaker interaction with $Bz^+$. Possibly, the signals marked by filled circles in Figure 4 arise from such isomers.

**D. $Bz^+-M_{1,2}$.** The $Bz^+-M$ spectrum displays a single broad band in the O−H stretch range centered at 3650 $cm^{-1}$ (Figure 4), which is assigned to the free O−H stretch of an H-bound dimer ($\nu_1^M$). Its structure is supposed to be similar to the one of $Bz^+-W$ shown in Figure 1a. The small red shift of −31 $cm^{-1}$ compared to free M ($\nu_1^M = 3681$ $cm^{-1}$)[57] confirms that the OH group of M is not involved in the formation of the intermolecular bond. The interaction in $Bz^+-M$ is expected to be slightly stronger than in $Bz^+-W$ because of the larger proton affinity of the ligand ($PA_M = 754.3$ kJ/mol, $PA_W = 691.0$ kJ/mol).[58] Consequently, the red shift in the O−H stretch is larger in $Bz^+-M$ (0.84%) than the average one in $Bz^+-W$ (0.78%).

In the C−H stretch range, the $Bz^+-M$ spectrum is richer than that of $Bz^+-W$ because of additional absorptions of the methyl group (Figure 5). The three C−H stretch fundamentals of isolated M occur at $\nu_2^M = 3000$, $\nu_3^M = 2844$, and $\nu_9^M = 2960$ $cm^{-1}$.[57] Bands H and G at 2965 and 3005 $cm^{-1}$ in the $Bz^+-M$ spectrum are attributed to $\nu_9^M$ and $\nu_2^M$ of the complex. The small complexation shifts indicate that, similar to the OH group, the $CH_3$ group of M is also not participating in intermolecular bonding. Interestingly, the intense $\nu_3^M$ mode of M is not observed for $Bz^+-M$, possibly because the presence of $Bz^+$ significantly reduces its IR intensity. Several $Bz^+-L$ examples are known for which $Bz^+$ complexation drastically changes the IR intensity of a certain ligand vibration.[30,31,44] Band C at 3090 $cm^{-1}$ in the $Bz^+-M$ spectrum is nearly unshifted from the corresponding $Bz^+-W$ transition and is readily assigned to the C−H stretch mode(s) of the $Bz^+$ moiety.

The signal-to-noise ratio of the $Bz^+-M_2$ spectrum obtained (not shown) is very low because of the large metastable background. Only the strongly IR active band F at 3655 $cm^{-1}$ is observed and assigned to the free O−H stretch ($\nu_1^M$) of isomer type I of $Bz^+-M_2$. This isomer has two single and (nearly) equivalent M ligands attached to $Bz^+$. Similar to $Bz^+-W_2$, the blue shift of $\Delta\nu_1^M = 5$ $cm^{-1}$ with respect to $Bz^+-M$ indicates that solvation of $Bz^+$ with the second ligand causes the interaction with the first ligand to become weaker. The magnitude of this noncooperative effect appears to be comparable in $Bz^+-M_2$ and $Bz^+-W_2$, resulting in similar blue shifts of the O−H stretch modes (≈5−6 $cm^{-1}$). Although isomer type II clusters of $Bz^+-M_2$ (an H-bonded $M_2$ dimer attached to $Bz^+$, similar to the structure in Figure 1e) may be present with significant abundance in the expansion, low signal levels prevent their spectroscopic identification in the present work.

## IV. Further Discussion

The IR spectra of $Bz^+-W(-N_2)$ in the O−H and C−H stretch ranges are consistent with the most stable $Bz^+-W$ structure shown in Figure 1a. This H-bound structure is mainly stabilized by charge−dipole interaction, and further contributions to the attraction arise from bifurcated H-bonding. No other $Bz^+-W$ isomer is detected. In contrast, the IR spectra of $Bz^+-W_n$ ($n = 2-4$) clearly show the presence of at least two classes of isomers. Type I corresponds to hydration of an interior $Bz^+$ cation and is described by $Bz^+-W_n$ geometries in which $n$ single W ligands are separately attached to $Bz^+$ (Figure 1d for $n = 2$). On the other hand, type II isomers are characterized by the formation of an H-bonded solvent network, because at least one W ligand forms an H-bond to another W ligand (Figure 1e for $n = 2$). Because the W−W interaction ($D_0 = 3.34 \pm 0.7$ kcal/mol)[49,50] is much weaker than the $Bz^+-W$ interaction ($D_0 = 14 \pm 3$ kcal/mol),[31] isomer type I should be more stable than isomer type II. As for C-bound and $\pi$-bound W ligands the interaction with $Bz^+$ is also stronger than the W−W bond, the most stable $Bz^+-W_n$ geometries are expected to be of type I even for large $n$; that is, an interior $Bz^+$ cation is completely solvated inside of a $W_n$ cluster.[24] However, the energy difference between both types of isomers seems to become signficantly

smaller as the cluster size increases, because further solvation affects the total binding energy in a noncooperative and cooperative fashion for isomer types I and II, respectively. Although the spectral data set for $Bz^+-M_n$ ($n \leq 2$) is smaller than for $Bz^+-W_n$ ($n \leq 4$), the principle cluster growth appears to be similar in both systems for small $n$. The $Bz^+-W$ interaction is slightly weaker than the $Bz^+-M$ interaction. A similar situation is observed for the related H-bonded dimers involving the phenol cation:[7,59−61] $D_0 = 18.54 \pm 0.11$ and 21.40 $\pm$ 0.18 kcal/mol for $Ph^+-W$ and $Ph^+-M$.[61]

The additional charge−dipole interaction significantly enhances the Bz−W interaction from $D_0 \approx 2.5$ kcal/mol in the $\pi$ H-bonded neutral dimer[22] to $D_0 = 14 \pm 3$ kcal/mol in the H-bound cation.[31] The large effect of ionization on the Bz−W interaction (energy and geometry) causes drastic differences between the cluster growth in $Bz^+-W_n$ and $Bz-W_n$, including the dimer geometry as well as the structure of the solvation shells. For neutral $Bz-W_n$, the solute−solvent (Bz−W) interaction is weaker than the solvent−solvent (W−W) interaction, leading to cluster structures in which Bz is surface solvated to a $W_n$ network (hydrophobic behavior of Bz). In contrast to the weak $\pi$ H-bond in neutral Bz−W, the charge−dipole bond of the $Bz^+-W$ cation is much stronger than the W−W interaction. Consequently, the most stable $Bz^+-W_n$ clusters (isomer type I) prefer interior $Bz^+$ solvation (hydrophilic behavior of $Bz^+$). In addition, the $W_n$ network in neutral $Bz-W_n$ differs from those in the type II isomers of $Bz^+-W_n$. Whereas in neutral $Bz-W_n$ a freely dangling H atom of a barely perturbed $W_n$ cluster is $\pi$ H-bonded to Bz, it is the O atom of the first W ligand that forms an H-bond to $Bz^+$ in $Bz^+-W_n$. Consequently, the water network in $Bz^+-W_n$ differs largely from bare $W_n$ clusters. Similar conclusions derived for the difference between $Bz-W_n$ and $Bz^+-W_n$ apply also to $Bz-M_n$ and $Bz^+-M_n$ and probably quite generally to bare neutral and cation aromatic hydrocarbon molecules interacting with polar solvents.

The often large difference between the structures of neutral and corresponding cation clusters has important consequences for the generation of cold cation clusters by photoionization.[11] For spectroscopic characterization, cation clusters are frequently produced by resonance enhanced multiphoton ionization (REMPI) of the neutral precursor. The Franck−Condon principle imposes severe restrictions on the REMPI process, and in many cases a given cation cluster cannot be produced in its most stable geometry but, for example, in a local minimum. In contrast, the electron impact (EI) ion source employed in the present work produces predominantly the most stable isomer of a cation dimer.[34−37,62] Thus, the IR spectra of cluster cations produced by EI and REMPI can be rather different.[34−37,62] Although the Bz−W and $Bz^+-W$ potentials are also quite different, the IR spectra of $Bz^+-W$ obtained by generating the complex in a REMPI and EI source are similar. In this particular case, REMPI of the $\pi$ H-bonded Bz−W leads to the generation of $Bz^+-W$ cations which mainly undergo dissociation.[63] However, a small fraction of $Bz^+-W$ isomerizes to the most stable H-bound structure shown in Figure 1a[22,28] and produces a REMPI−IR spectrum[30] similar to the EI−IR spectrum.[31] Nonetheless, the Franck−Condon restrictions in the REMPI process have led to a wrong determination of the $Bz^+-W$ dissociation energy[64] because of an ill-determined adiabatic ionization potential.[22,31] Although the REMPI−IR and EI−IR spectra of the $Bz^+-W$ dimer are similar, it will be interesting to explore whether comparable spectra are also observed for larger $Bz^+-W_n$ clusters because of the different production pathways. In the EI source, Bz is first ionized and subsequently W ligands are attached to the ion ("pickup") in several different reaction steps, as described by eq 1(a−d). In the REMPI ion source, neutral $Bz-W_n$ complexes are first formed and then ionized, similar to eq 2. The generated $Bz^+-W_n$ ions will then undergo some structural rearrangement and possibly evaporative and/or collisional cooling. Thus, different $Bz^+-W_n$ cluster isomers may be produced by the EI and REMPI ion sources for $n > 1$, providing complementary information about global and local minimum structures.

Comparison of $Bz^+-L_n$ (L = W, M) with corresponding clusters of the phenol and aniline cations ($Ph^+-L_n$, $An^+-L_n$)[7,9,55,59−61,65−69] reveals the effect of substitution of acidic functional groups (OH, $NH_2$) on the solvation of an aromatic hydrocarbon cation by polar ligands. The $Ph^+-L$ and $An^+-L$ dimers feature nearly linear H-bonds between the protons of the polar group and the O atom of L = W and M. These charge−dipole structures are similar to the corresponding H-bound $Bz^+-L$ dimers, with the main difference being that the polar group enhances the interaction strength. All spectroscopic data for larger $Ph^+-L_n$ ($n \leq 8$ for L = W, $n \leq 1$ for L = M)[7,9,55,59−61,65−67] and $An^+-W_n$ ($n \leq 6$ for L = W, $n \leq 2$ for L = M)[68,69] clusters have been interpreted with geometries in which the ligands solvate the polar group; that is, the aromatic ion is surface solvated to the $L_n$ network. No evidence was presented for isomers in which a ligand is attached to the aromatic ring (as in Figure 1a−c). This is in striking contrast to the $Bz^+-L_n$ spectra discussed in the present work. Consequently, one may conclude that substitution with a polar group has a drastic effect on the competition between interior solvation of the aromatic cation and the formation of the H-bonded $L_n$ network. On the other hand, one has to bear in mind that the studies of the $Ph^+-L_n$ and $An^+-L_n$ clusters with larger $n$ used REMPI ionization,[55,69] which may not necessarily produce the most stable cluster ion structures. Moreover, in the case of $Ph^+-W_n$, proton transfer from $Ph^+$ to the $W_n$ network was observed for $n \geq 3-4$.[9,55,66,67]

Aromatic cations are known to be highly reactive in aqueous solution. The proton affinity of the phenyl radical is much higher than those of W and M (PA = 691, 754, and 884 kJ/mol for W, M, and $C_6H_5$).[58] Moreover, the ionization potential of Bz is lower than those of W and M (IP = 9.2, 10.9, and 12.6 eV for Bz, M, and W).[70] Consequently, in the most stable $Bz^+-L$ (L = W, M) dimers the positive charge is largely localized in $Bz^+$ and proton transfer from $Bz^+$ to L is not observed. The PA of larger $L_n$ clusters increases with $n$, whereas the IP decreases. Hence, both proton and charge transfer from $Bz^+$ to $L_n$ become less endothermic for increasing $n$ and at a certain cluster size intracluster reactions can occur. Indeed, charge and proton transfer was observed in $Bz^+-M_n$ after photoionization for $n \geq 3$ and $n \geq 4$, respectively.[33] Similarly, proton transfer was observed in $Bz^+-W_n$ in the size range $n = 20-30$.[24] Due to the lower PA and higher IP, water is a less reactive solvent than methanol. The present IR spectroscopic fragmentation experiments confirm that $Bz^+-L_n$ produced in the EI ion source are unreactive in the size ranges $n \leq 3$ (L = W) and $n = 1$ (L = M), respectively. The missing band E in the $Bz^+-W_4$ spectrum may be taken as evidence that proton transfer actually may occur for this cluster size.[71] Again, it should be noted that the REMPI and EI ion sources usually produce different cluster isomers which exhibit different intracluster reactivity. Future EI−IR spectroscopic experiments on larger clusters may shed further light on the cluster size dependence of different reaction channels (proton and charge transfer). Moreover, analysis of the wavelength and mode dependence of laser-induced reactions

in $Bz^+-L_n$ may provide deeper insight into the energetics of these ion−molecule reactions (e.g., barrier heights) as well as the possibility to investigate mode-selective chemistry.

## V. Concluding Remarks

The IR spectra of $Bz^+-L_n$ ($n \leq 4$ for L = W, $n \leq 2$ for L = M) recorded in the present work correspond to the first spectroscopic effort to investigate the stepwise microsolvation process of an aromatic hydrocarbon cation by polar ligands. The $Bz^+-L$ dimer spectra are consistent with H-bound charge−dipole equilibrium structures, in which L approaches $Bz^+$ in the aromatic plane to form two H-bonds between the lone pairs of the O atom of L and adjacent protons of $Bz^+$. Only one isomer is observed for the $Bz^+-L$ dimers, whereas clearly two classes of isomers are identified for larger $Bz^+-L_n$ clusters through spectral analysis in the O−H stretch range. Class I isomers of $Bz^+-L_n$ correspond to solvation of an interior $Bz^+$ cation by $n$ solvent molecules via charge−dipole H-bonds (Figure 1d for $n = 2$). Although the ligands are probably equivalent in this type of isomers, the average binding energy of the ligands tends to decrease as $n$ increases. Such noncooperative effects are quite common for solvation of organic and inorganic ions by polar ligands.[72] The class II isomers of $Bz^+-L_n$ identified are characterized by the formation of an H-bonded ligand network; that is, at least two ligands are connected via an H-bond (Figure 1e for $n = 2$). Apparently, the presence of the $Bz^+$ cation increases the strength of the H-bonds within this network through cooperative three-body effects. As the $Bz^+-L$ interaction exceeds by far the L−L interaction, class I isomers are probably more stable than class II isomers. However, both isomer types are produced with significant abundance in the EI cluster ion source because of the various competing reaction sequences for the cluster growth, which are controlled by both thermodynamic and kinetic factors. Although the data set for $Bz^+-M_n$ ($n \leq 2$) is smaller compared to $Bz^+-W_n$ ($n \leq 4$), the deduced picture of the microsolvation process appears to be similar in both systems in the size range investigated. In general, the $Bz^+-M$ bond is stronger than the $Bz^+-W$ bond, because of the higher proton affinity of M. Although a crude picture of the competition between $Bz^+$ solvation and the formation of a solvent network could be established through the analysis of the mid-IR spectra, high-level quantum calculations are required to determine accurate geometries and stabilization energies of the various possible isomers of $Bz^+-L_n$. Moreover, higher quality spectroscopic data (e.g., from double resonance spectroscopies) may help to distinguish unambiguously between signals originating from different $Bz^+-L_n$ isomers. Comparison between $Bz^+-L_n$ and the corresponding neutral $Bz-L_n$ complexes reveals that ionization of the aromatic solute has a massive effect on both the dimer potential (interaction strength and equilibrium geometry) as well as the structure of solvation shells.

**Acknowledgment.** This study is part of project No. 20-63459.00 of the Swiss National Science Foundation. O.D. is supported by the Deutsche Forschungsgemeinschaft via a Heisenberg Fellowship (DO 729/1-1). The authors acknowledge fruitful discussions with Dr. A. Fujii on the properties of $Bz^+-W_n$.

## References and Notes

(1) Hobza, P.; Zahradnik, R. *Intermolecular Complexes: The Role of van der Waals Systems in Physical Chemistry and in the Biodisciplines*; Elsevier: Amsterdam, 1988.
(2) Jeffrey, G. A.; Saenger, W. *Hydrogen Bonding in Biological Systems*; Springer: Heidelberg, 1991.
(3) Teeter, M. M. *Annu. Rev. Biophys. Biophys. Chem.* **1991**, *20*, 577.
(4) Stryer, L. *Biochemistry*; Freeman: New York, 1996.
(5) *Chem. Rev.* **1994**, *94*(7), 4. *Chem. Rev.* **2000**, *100*(11).
(6) Bieske, E. J.; Dopfer, O. *Chem. Rev.* **2000**, *100*, 3963.
(7) Müller-Dethlefs, K.; Dopfer, O.; Wright, T. G. *Chem. Rev.* **1994**, *94*, 1845.
(8) Müller-Dethlefs, K.; Hobza, P. *Chem. Rev.* **2000**, *100*, 143.
(9) Ebata, T.; Fujii, A.; Mikami, N. *Int. Rev. Phys. Chem.* **1998**, *17*, 331.
(10) Zwier, T. S. *Annu. Rev. Phys. Chem.* **1996**, *47*, 205.
(11) Brutschy, B. *Chem. Rev.* **2000**, *100*, 3891.
(12) Pribble, R. N.; Zwier, T. S. *Science* **1994**, *265*, 75.
(13) Zwier, T. S. *Advances in Molecular Vibrations and Collision Dynamics* **1998**, *3*, 249.
(14) Suzuki, S.; Green, P. G.; Bumgarner, R. E.; Dasgupta, S.; Goddard, W. A., III; Blake, G. A. *Science* **1992**, *257*, 942.
(15) Gutowski, H. S.; Emilsson, T.; Arunan, E. *J. Chem. Phys.* **1993**, *99*, 4883.
(16) Maxton, P. M.; Schaeffer, M. W.; Ohline, S. M.; Kim, W.; Venturo, V. A.; Felker, P. M. *J. Chem. Phys.* **1994**, *101*, 8391.
(17) Tarakeshwar, P.; Choi, H. S.; Lee, S. J.; Lee, J. Y.; Kim, K. S.; Ha, T.-K.; Jang, J. H.; Lee, J. G.; Lee, H. *J. Chem. Phys.* **1999**, *111*, 5838.
(18) Feller, D. *J. Phys. Chem. A* **1999**, *103*, 7558.
(19) Fredericks, S. Y.; Jordan, K. D.; Zwier, T. S. *J. Phys. Chem.* **1996**, *100*, 7810.
(20) Gregory, J. K.; Clary, D. C. *Mol. Phys.* **1996**, *88*, 33.
(21) Kim, K. S.; Tarakeshwar, P.; Lee, J. Y. *Chem. Rev.* **2000**, *100*, 4145.
(22) Courty, A.; Mons, M.; Dimicoli, I.; Piuzzi, F.; Gaigeot, M.-P.; Brenner, V.; de Pujo, P.; Millie, P. *J. Phys. Chem. A* **1998**, *102*, 6590.
(23) Gruenloh, C. J.; Carney, J. R.; Hagemeister, F. C.; Zwier, T. S.; Wood, J. T., III; Jordan, K. D. *J. Chem. Phys.* **2000**, *113*, 2290.
(24) Courty, A.; Mons, M.; Le Calve, J.; Piuzzi, F.; Dimicoli, I. *J. Phys. Chem. A* **1997**, *101*, 1445.
(25) Tschumper, G. S.; Leininger, M. L.; Hoffman, B. C.; Valeev, E. F.; Schaefer, H. F., III; Quack, M. *J. Chem. Phys.* **2002**, *116*, 690.
(26) Pribble, R. N.; Hagemeister, F. C.; Zwier, T. S. *J. Chem. Phys.* **1997**, *106*, 2145.
(27) Gruenloh, C. J.; Florio, G. M.; Carney, J. R.; Hagemeister, F. C.; Zwier, T. S. *J. Phys. Chem. A* **1999**, *103*, 496.
(28) Tachikawa, H.; Igarashi, M. *J. Phys. Chem. A* **1998**, *102*, 8648.
(29) Tachikawa, H.; Igarashi, M.; Ishibashi, T. *Phys. Chem. Chem. Phys.* **2001**, *3*, 3052.
(30) Miyazaki, M.; Fujii, A.; Ebata, T.; Mikami, N. *Chem. Phys. Lett.* **2001**, *349*, 431.
(31) Solcà, N.; Dopfer, O. *Chem. Phys. Lett.* **2001**, *347*, 59.
(32) Stone, A. J. *The theory of intermolecular forces*; Clarendon Press: Oxford, 1996.
(33) Garrett, A. W.; Zwier, T. S. *J. Chem. Phys.* **1992**, *96*, 7259.
(34) Solcà, N.; Dopfer, O. *J. Phys. Chem. A* **2001**, *105*, 5637.
(35) Solcà, N.; Dopfer, O. *Chem. Phys. Lett.* **2000**, *325*, 354.
(36) Solcà, N.; Dopfer, O. *Eur. Phys. J. D* **2002**, *20*, 469.
(37) Solcà, N.; Dopfer, O. *J. Phys. Chem. A* **2002**, *106*, 7261.
(38) NIST Chemistry WebBook (National Institute of Standard and Technology, Gaithersburg, http://webbook.nist.gov).
(39) Zhong, W.; Nikolaev, E. N.; Futrell, J. H.; Wysocki, V. H. *Anal. Chem.* **1997**, *69*, 2496.
(40) Guelachvili, G.; Rao, K. N. *Handbook of Infrared Standards*; Academic Press: London, 1993.
(41) Camy-Peyret, C.; Flaud, J. M.; Guelachvili, G.; Amiot, C. *Mol. Phys.* **1973**, *26*, 825.
(42) Herzberg, G. *Molecular Spectra and Molecular Structure. II. Infrared and Raman Spectra of Polyatomic Molecules.*; Krieger Publishing Company: Malabar, Florida, 1991.
(43) Pribble, R. N.; Garrett, A. W.; Haber, K.; Zwier, T. S. *J. Chem. Phys.* **1995**, *103*, 531.
(44) Dopfer, O.; Olkhov, R. V.; Maier, J. P. *J. Chem. Phys.* **1999**, *111*, 10754.
(45) Fujii, A.; Fujimaki, E.; Ebata, T.; Mikami, N. *J. Chem. Phys.* **2000**, *112*, 6275.
(46) Bakker, J. M.; Satink, R. G.; von Helden, G.; Meijer, G. *Phys. Chem. Chem. Phys.* **2002**, *4*, 24.
(47) Huang, Z. S.; Miller, R. E. *J. Chem. Phys.* **1989**, *91*, 6613.
(48) Dyke, T. R.; Mack, K. M.; Muenter, J. S. *J. Chem. Phys.* **1977**, *66*, 498.
(49) Curtiss, L. A.; Frurip, D. J.; Blander, M. *J. Chem. Phys.* **1979**, *71*, 2703.
(50) Mas, E. M.; Bukowski, R.; Szalewicz, K.; Groenenboom, G. C.; Wormer, P. E. S.; van der Avoird, A. *J. Chem. Phys.* **2000**, *113*, 6687.
(51) Lindner, R.; Müller-Dethlefs, K.; Wedum, E.; Haber, K.; Grant, E. R. *Science* **1996**, *271*, 1698.

(52) Müller-Dethlefs, K.; Peel, J. B. *J. Chem. Phys.* **1999**, *111*, 10550.
(53) Applegate, B.; Miller, T. A. *J. Chem. Phys.* **2002**, *117*, 10654.
(54) Huisken, F.; Kaloudis, M.; Kulcke, A. *J. Chem. Phys.* **1996**, *104*, 17.
(55) Kleinermanns, K.; Janzen, C.; Spangenberg, D.; Gerhards, M. *J. Phys. Chem. A* **1999**, *103*, 5232.
(56) Ludwig, R. *Angew. Chem., Int. Ed.* **2001**, *40*, 1808 and references therein.
(57) Shimanouchi, T. *Tables of Molecular Vibrational Frequencies, Consolidated Volume I*; National Standard Reference Data Series−National Bureau of Standards: Washington, DC, 1972; Vol. 39.
(58) Hunter, E. P. L.; Lias, S. G. *J. Phys. Chem. Ref. Data* **1998**, *27*, 413.
(59) Dopfer, O.; Reiser, G.; Müller-Dethlefs, K.; Schlag, E. W.; Colson, S. D. *J. Chem. Phys.* **1994**, *101*, 974.
(60) Wright, T. G.; Cordes, E.; Dopfer, O.; Müller-Dethlefs, K. M. *J. Chem. Soc., Faraday Trans.* **1993**, *89*, 1609.
(61) Courty, A.; Mons, M.; Dimicoli, I.; Piuzzi, F.; Brenner, V.; Millie, P. *J. Phys. Chem. A* **1998**, *102*, 4890.
(62) Solcà, N.; Dopfer, O. *J. Mol. Struct.* **2001**, *563/564*, 241.
(63) Gotch, A. J.; Zwier, T. S. *J. Chem. Phys.* **1992**, *96*, 3388.
(64) Cheng, B.-M.; Grover, J. R.; Walters, E. A. *Chem. Phys. Lett.* **1995**, *232*, 364.
(65) Sawamura, T.; Fujii, A.; Sato, S.; Ebata, T.; Mikami, N. *J. Phys. Chem.* **1996**, *100*, 8131.
(66) Ebata, T.; Fujii, A.; Mikami, N. *Int. J. Mass Spectrosc. Ion Proc.* **1996**, *159*, 111.
(67) Sato, S.; Mikami, N. *J. Phys. Chem.* **100**, *100*, 4765.
(68) Honkawa, Y.; Inokuchi, Y.; Ohashi, K.; Nishi, N.; Sekiya, H. *Chem. Phys. Lett.* **2002**, *358*, 419.
(69) Nakanaga, T.; Ito, F. *Chem. Phys. Lett.* **2001**, *348*, 270.
(70) Lias, S. G.; Barmess, J. E.; Liebman, J. F.; Holmes, J. L.; Levin, R. D.; Mallard, W. G. *J. Phys. Chem. Ref. Data Suppl.* **1988**, *17*, 1.
(71) A. Fujii, private communication, 2002.
(72) Keesee, R. G.; Castleman, A. W., Jr. *J. Phys. Chem. Ref. Data* **1986**, *15*, 1011.
(73) Fujii, A.; Fujimaki, E.; Ebata, T.; Mikami, N. *Chem. Phys. Lett.* **1999**, *303*, 289.